ARTICLES

Full-folding optical potentials in elastic proton-nucleus scattering

Ch. Elster
Department of Physics, The Ohio State University, Columbus, Ohio 43210

Taksu Cheon and Edward F. Redish
Department of Physics and Astronomy, University of Maryland, College Park, Maryland 20742

P. C. Tandy
Department of Physics, Kent State University, Kent, Ohio 44242

(Received 11 September 1989)

The optical potential for elastic scattering of protons from ^{16}O at incident beam energies between 100 and 500 MeV is calculated from a full-folding integral of a simple *s-p*-shell representation of the target density matrix together with fully off-shell nucleon-nucleon *t* matrices derived from two different Bonn meson exchange models. Elastic scattering observables calculated from this full-folding optical potential are compared to those obtained from "optimum factorized" as well as on-shell local ("*tρ*") approximations. The optimum factorization is found to provide a good approximation to elastic scattering observables obtained from the full-folding optical potential, although the potentials differ in the structure of their nonlocality. A perturbative treatment of the nonlocality is used to extract approximate localized potentials and associated Perey damping factors for the interior wave functions. The results indicate that the interior wave function from the optimum factorization potential and the full-folding potential are very similar.

I. INTRODUCTION

The theory of the nucleon-nucleus optical potential continues to play an important role in modern nuclear physics. The motivation for ongoing work on this topic is twofold. First, elastic and inelastic nucleon-nucleus scattering seem to provide an important and sensitive test for theoretical corrections at the first-order level of the optical potential given by relativistic dynamics,[1,2] medium modifications of the nucleon-nucleon interaction,[3] and off-shell effects.[4–6] Second, high-energy coincidence experiments will be extremely important in the next decade and the wave functions needed for continuum nucleons in the interior of the nucleus will require a better understanding of the theoretical optical potential than is necessary for just the elastic observables.

There have been extensive analyses of relativistic models which appear to show that it is more appropriate to treat the nucleon as a relativistic Dirac particle than as a nonrelativistic Pauli particle. Indeed, it has been suggested that these tests, among others, strongly indicate that our underlying theory of nuclei should be relativistic. If our analysis of intermediate energy scattering is to provide that strong a lever on our view of nuclear physics, we must proceed with considerable caution and be certain that we understand in detail the corrections to our calculations of the optical potential, both relativistic and nonrelativistic. There are already strong indications that some models of effective interactions that are assumed to produce good representations of nonrelativistic methods have some very inconsistent features.[7] Calculations using these models to "test nonrelativistic theory" may not, in fact, do so, and conclusions based on the inadequacy of the nonrelativistic approach may be premature.[2]

In the next decade, a number of important high-energy coincidence experiments are planned with weak or electromagnetic probes. In these experiments, a probe particle (electron or neutrino) will interact with a nucleon inside the nucleus and knock it out. The struck particle will then be observed, in some cases in coincidence with the scattered projectile. The inference from these experiments of the behavior of nucleons within the nucleus may have important implications for our understanding of nucleonic as well as nuclear structure. However, the "source" for the "beam" of nucleons that we will detect will in fact be inside the nucleus. In order to extract any information about how the fundamental process is modified inside the nucleus, we will have to understand how the struck nucleon interacts with the nucleus on its way out. This is not a trivial extension of optical model theory. Our current tests of the optical potential are mostly based on elastic scattering which is not very sensitive to what is happening in the nuclear interior. In order to interpret knockout experiments, we will need to have a much better understanding of optical potential mechanisms than we do now.

In this paper we consider one of the corrections to the single-scattering nonrelativistic theory of the optical potential: the effect of full-folding. The single-scattering optical potential is given by the triangle graph shown in Fig. 1. Since there is one loop, the graph requires a three-dimensional integration involving a fully-off-shell two-nucleon scattering amplitude and the nuclear density matrix. [See Eq. (2)]. Usually, one makes the assumption that the nucleon-nucleon amplitude varies slowly as a function of its arguments compared to the nuclear densi-

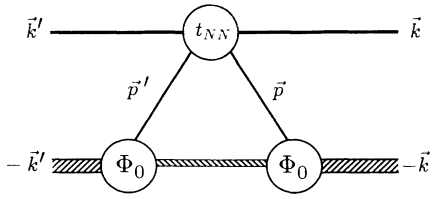

FIG. 1. Diagram for the optical potential matrix element for the single-scattering approximation.

ty matrix. This corresponds to the argument that the range of the nucleon-nucleon force is small compared to the size of the nucleus and leads to the approximate nonrelativistic form $t(q)\rho(q)$ for the first-order nucleon-nucleus optical potential.

This is an appealing starting point, because both the on-shell nucleon-nucleon (NN) scattering amplitude t and the one-nucleon density ρ for the target nucleus can be obtained from independent experiments. It is also convenient because it is local and thus serves as a basis for a large body of phenomenological work. The underlying assumption leading to the local $t(q)\rho(q)$ form is certainly approximately correct and higher-order effects at forward scattering angles relate to the energy derivative of t.[8] However, intermediate-energy nucleon-nucleus elastic scattering is highly sensitive to details, especially the spin dependence of scattering near interference minima. Therefore, it is necessary to investigate the effect of the range of the two-nucleon force on the momentum nonlocality in an appropriate fashion and perform the integration indicated in the triangle graph of Fig. 1.

The purpose of this paper is to test in a simple model the accuracy of commonly used approximations to the full-folding calculation, namely the local on-shell and the optimum factorized off-shell approximation.[4,9,10] Also, approximate expansions, which have been developed to obtain an effective local form,[11] can be tested for their ability to capture the dominant nonlocal effects. We construct the full-folding optical potential after a method proposed by Redish and Stricker-Bauer (RSB).[12] This method is based on the observation that the fully-off-shell central and spin-orbit nucleon-nucleon amplitudes appear to simplify, when their momentum dependence is expressed in terms of an appropriate set of variables. In the case that the nuclear density matrix can be expanded in terms of harmonic oscillator functions, the full-folding integral can be partly performed analytically. Preliminary results for the matrix elements of the resulting optical potential based on the Reid Soft Core potential as two-nucleon input were shown in Ref. 13.

In this paper we construct the full-folding single-scattering optical potential for ^{16}O using a two-parameter harmonic oscillator density matrix for closed s and p shells and the fully-off-shell nucleon-nucleon scattering amplitudes from the full Bonn meson exchange model[14] at 200 MeV and from one of its derivatives[6] at 500 MeV scattering energy. We find that the off-shell optimum factorization provides a very good approximation for both the elastic scattering observables as well as the interior damping[15] of the wave function, especially at higher energies. The investigations carried out here have many similarities to a recent study[16] of the full-folding optical potential for ^{40}Ca based upon the t matrix derived from the Paris Potential. In particular the qualitative nature of the effects upon the spin observables reported here agrees with the ones found in Ref. 16.

The structure of the paper is as follows. In Sec. II we review the formalism for the single-scattering optical potential and the RSB method. In Sec. III, we discuss the harmonic oscillator model employed for the density matrix. The calculations of the full-folding optical potential are carried out in Sec. IV and the resulting potentials are displayed. We discuss the elastic scattering results in Sec. V. In Sec. VI we carry out an approximate localization of the nonlocal potentials and extract Perey damping factors for the interior wave functions to provide a characterization of the dominant effect. Our conclusions are presented in Sec. VII.

II. THE FIRST-ORDER OPTICAL POTENTIAL

In the nonrelativistic multiple-scattering theory of Kerman, McManus, and Thaler,[17] the first-order optical potential may be expressed as

$$\langle \mathbf{k}'|U(E)|\mathbf{k}\rangle = \left[\frac{A-1}{A}\right]\left\langle \mathbf{k}'\Phi_0\left|\sum_{\alpha=p,n} t_\alpha(\varepsilon)\right|\mathbf{k}\Phi_0\right\rangle . \quad (1)$$

Here $t_\alpha(\varepsilon)$ is the free NN t matrix at an appropriate energy ε. In principle, this energy should be the beam energy minus the kinetic energy of the center of mass of the interacting pair less the binding energy of the struck particle.[18] Thus ε is coupled to the integration variable. In practice, the relevant matrix elements of t do not depend strongly on this variable,[18] so we will fix it at the two-body c.m. energy corresponding to free NN scattering at the beam energy. This corresponds to ignoring the effect of the binding correction and Fermi motion on the energy shift. The momenta $\mathbf{k}'$ and $\mathbf{k}$ are the final and initial momenta of the projectile in the frame of zero total nucleon-nucleus momentum, respectively. The effect of Fermi motion upon the effective NN relative momenta is retained, however.

With insertion of complete sets of momenta for the struck target nucleon before and after the collision, we get the following explicit expression for the optical potential in momentum space:

$$\langle \mathbf{k}'|U(E)|\mathbf{k}\rangle = \left[\frac{A-1}{A}\right]\sum_{\alpha=p,n}\int \frac{d^3\mathbf{p}'}{(2\pi)^3}\frac{d^3\mathbf{p}}{(2\pi)^3}\left\langle \frac{\mathbf{k}'-\mathbf{p}'}{2}|t_\alpha(\varepsilon)|\frac{\mathbf{k}-\mathbf{p}}{2}\right\rangle \rho_\alpha(\mathbf{p}',\mathbf{p})\delta(\mathbf{k}'+\mathbf{p}'-\mathbf{k}-\mathbf{p}) . \quad (2)$$

Recoil effects have been ignored. The density matrices ρ_p and ρ_n are normalized to the number of protons and neutrons, respectively. The integrations over the initial and final momenta of the target nucleon are reduced to a single

momentum integration by the conservation of the total two-nucleon momentum by the two-body interaction. If $U(E)$, $t_\alpha(\varepsilon)$, and ρ are rewritten as functions of the difference and average of their momentum arguments and one integration is performed, Eq. (2) becomes

$$\langle \mathbf{k}'|U(E)|\mathbf{k}\rangle \equiv \tilde{U}(\mathbf{q},\mathbf{K}) = \left[\frac{A-1}{A}\right] \sum_{\alpha=p,n} \int \frac{d^3\mathbf{P}}{(2\pi)^3} \tilde{t}_\alpha \left[\mathbf{q}, \frac{\mathbf{K}-\mathbf{P}}{2}; \varepsilon\right] \tilde{\rho}_\alpha(\mathbf{q},\mathbf{P}) . \tag{3}$$

The tilde indicates a function of initial and final momenta and has been expressed as a function of the difference and average of those momenta, that is,

$$\tilde{f}(\mathbf{k}'-\mathbf{k},(\mathbf{k}'+\mathbf{k})/2) = f(\mathbf{k}',\mathbf{k}) .$$

Explicitly, the momenta in Eq. (3) are defined by $\mathbf{q}=\mathbf{k}'-\mathbf{k}$, $\mathbf{K}=(\mathbf{k}'+\mathbf{k})/2$, and $\mathbf{P}=(\mathbf{p}'+\mathbf{p})/2$.

Common approximations to the full-folding expression in Eq. (3) are obtained as follows. If we observe that the nuclear size is significantly larger than the range of the *NN* interaction, the two-body t-matrix $\tilde{t}_\alpha$ is expected to be the most slowly varying factor in Eq. (3). This argues for the method of optimum factorization,[9,10] which proceeds via an expansion of $\tilde{t}_\alpha$ in a Taylor series in $\mathbf{P}$ about a fixed value $\mathbf{P}_0$. The reference momentum $\mathbf{P}_0$ is determined by requiring that the contribution of the first derivative term be minimized. In the present elastic scattering case, this contribution can be made to vanish if $\mathbf{P}_0$ is chosen to be zero. For further details we refer to Ref. 4.

After integration over the density matrix to produce the diagonal one-body density, the optimum factorized approximation for the optical potential is

$$\tilde{U}_{\rm fac}(\mathbf{q},\mathbf{K}) = \left[\frac{A-1}{A}\right] \sum_{\alpha=p,n} \tilde{t}_\alpha \left[\mathbf{q}, \frac{\mathbf{K}}{2}; \varepsilon\right] \tilde{\rho}_\alpha(q) . \tag{4}$$

Since $\mathbf{q}$ and $\mathbf{K}$ are arbitrary and not related to the on-shell value of the two-body t matrix, we refer to $\tilde{U}_{\rm fac}$ as an "off-shell $t\rho$" approximation. If we further assume that for any $\mathbf{K}$ the two-body t-matrix $\tilde{t}_\alpha(\mathbf{q},\mathbf{K}/2;\varepsilon)$ in Eq. (4) is equal to its on-shell value $\tilde{t}_\alpha^{\rm on}(\mathbf{q};\varepsilon)$, we obtain the local "$t\rho$" approximation. This involves the replacement of $\mathbf{K}$ in Eq. (4) by the value calculated from the on-shell conditions $\mathbf{q}\cdot\mathbf{K}=0$ and $\mathbf{q}^2+\mathbf{K}^2=4\mathbf{k}_0^2$, with $\mathbf{k}_0$ being the on-shell relative momentum for *NN* scattering at energy ε. Since the new value of $\mathbf{K}$ is determined completely by the argument $\mathbf{q}$ in $\tilde{U}_{\rm fac}$ at a given energy ε, the potential becomes independent of the variable $\mathbf{K}$ and thus is local. Explicitly, we have the on-shell or local approximation:

$$\tilde{U}_{\rm on}(\mathbf{q},\mathbf{K}) = \left[\frac{A-1}{A}\right] \sum_{\alpha=p,n} \tilde{t}_\alpha(q)\tilde{\rho}_\alpha(q) . \tag{5}$$

Our principal concern in this work is the evaluation of Eq. (3). In general, this three-dimensional integration is complicated due to angular dependence of both the off-shell t matrix and the target density matrix in the momentum variables. Off-shell effects from the t matrix have been found to be quite important when the optimum factorization in Eq. (4) is employed.[4,6,13] For this reason we wish to evaluate the full-folding integration of Eq. (3) in the context of a simple model for the density matrix $\tilde{\rho}_\alpha(\mathbf{q},\mathbf{P})$ while retaining the full off-shell structure of the t matrix. With a harmonic oscillator model for the target, the density matrix depends only on the magnitudes q and P and the task is considerably simplified. It is convenient to apply the variable change $\mathbf{Q}=(\mathbf{K}-\mathbf{P})/2$ so that Eq. (3) becomes

$$\tilde{U}(\mathbf{q},\mathbf{K}) = 8\left[\frac{A-1}{A}\right] \sum_{\alpha=p,n} \int \frac{d^3\mathbf{Q}}{(2\pi)^3} \tilde{t}_\alpha(\mathbf{q},\mathbf{Q}) \times \tilde{\rho}_\alpha(q,|\mathbf{K}-2\mathbf{Q}|) . \tag{6}$$

The momentum $\mathbf{Q}$ is the average of the initial and final relative momenta of the two active nucleons, and the t matrix has a very simple orientational dependence in the variables shown. As detailed in Sec. IV, the two angular integrations can be performed analytically in the case of an oscillator density matrix leaving a one-dimensional numerical quadrature to complete the full-folding integral.

III. DENSITY MATRIX FOR ^{16}O

Since our goal is to test the accuracy of approximations to the full-folding integral rather than to make a detailed comparison with data, we choose to consider the scattering from the closed-shell nucleus ^{16}O with the assumption of occupied s and p shells only. We approximate the density matrix by two harmonic oscillator terms. The one particle s-wave harmonic oscillator wave function is given by (the notation is Ψ_{nlm})

$$\Psi_{000}(p) = (2\pi)^{3/2}\left[\frac{4}{\sqrt{\pi}\nu_s^{3/2}}\right]^{1/2} \frac{1}{\sqrt{4\pi}} e^{-p^2/2\nu_s} \tag{7}$$

and the one-particle p-wave function by

$$\Psi_{01m}(p) = (2\pi)^{3/2}\left[\frac{4}{\sqrt{\pi}\nu_p^{3/2}}\right]^{1/2} \sqrt{\tfrac{2}{3}}\frac{p}{\sqrt{\nu_p}} \times e^{-p^2/2\nu_p} \mathcal{Y}_{1m}(\hat{p}) . \tag{8}$$

The s-shell contribution to the density matrix is therefore

$$\rho_{00}(p,p') = \Psi_{000}^*(p')\Psi_{000}(p) = \left[\frac{4\pi}{\nu_s}\right]^{3/2} e^{-(p'^2+p^2)/2\nu_s} . \tag{9}$$

With the change of variables, $\mathbf{q}=\mathbf{p}-\mathbf{p}'$ and $\mathbf{P}=(\mathbf{p}+\mathbf{p}')/2$, we obtain

$$\tilde{\rho}_{00}(q,P) = \left[\frac{4\pi}{\nu_s}\right]^{3/2} e^{-(P^2/\nu_s+q^2/4\nu_s)} . \tag{10}$$

The p-shell contribution to the density matrix is

$$\rho_{01}(p',p)=\tfrac{1}{3}\sum_m \Psi^*_{01m}(p')\Psi_{01m}(p) . \tag{11}$$

This becomes explicitly

$$\tilde{\rho}_{01}(q,P)=\frac{2}{3}\left[\frac{4\pi}{\nu_p}\right]^{3/2}(P^2/\nu_p-q^2/4\nu_p) \times e^{-(P^2/\nu_p+q^2/4\nu_p)} \tag{12}$$

after use is made of the property

$$\sum_m pp'\mathcal{Y}_{1m}(\hat{p}')\mathcal{Y}_{1m}(\hat{p})=(3/4\pi)\mathbf{p}'\cdot\mathbf{p}$$

satisfied by spherical harmonics. The density matrix for ^{16}O in this harmonic oscillator model is then given by

$$\tilde{\rho}(q,P)=4\tilde{\rho}_{00}(q,P)+12\tilde{\rho}_{01}(q,P) . \tag{13}$$

It should be noted that due to the special choice of harmonic oscillator wave functions the density $\tilde{\rho}(q,P)$ depends only on the magnitudes of **q** and **P**. The diagonal density $\tilde{\rho}(q)$ is obtained by integrating over **P**, i.e.,

$$\tilde{\rho}(q)=\int \frac{d^3\mathbf{P}}{(2\pi)^3}\tilde{\rho}(q,P) . \tag{14}$$

The insertion of Eqs. (10), (12), and (13) into this expression leads to the simple result

$$\tilde{\rho}(q)=4e^{-\beta_s}+12(1-\tfrac{2}{3}\beta_p)e^{-\beta_p} , \tag{15}$$

where we have used the abbreviations $\beta_{s,p}=q^2/4\nu_{s,p}$. We determine the oscillator parameters ν_s and ν_p by fitting the diagonal density of Eq. (15) to a three-parameter Fermi shape density which describes the experimentally determined proton charge distribution obtained from electron scattering up to about 4 fm^{-1}.[19]

In Fig. 2 the Fourier transform of the Fermi shape density distribution is represented by the dashed line. Our best fit to the density with harmonic oscillator wave functions is given by the solid line. We obtain the oscillator parameters $\nu_s=0.310$ fm^{-2} and $\nu_p=0.336$ fm^{-2}. The curve from the first peak at $q=0$ down to the zero in ρ in the neighborhood of $q=1.6$ fm^{-1} is excellently described by the oscillator model. However, the enlarged

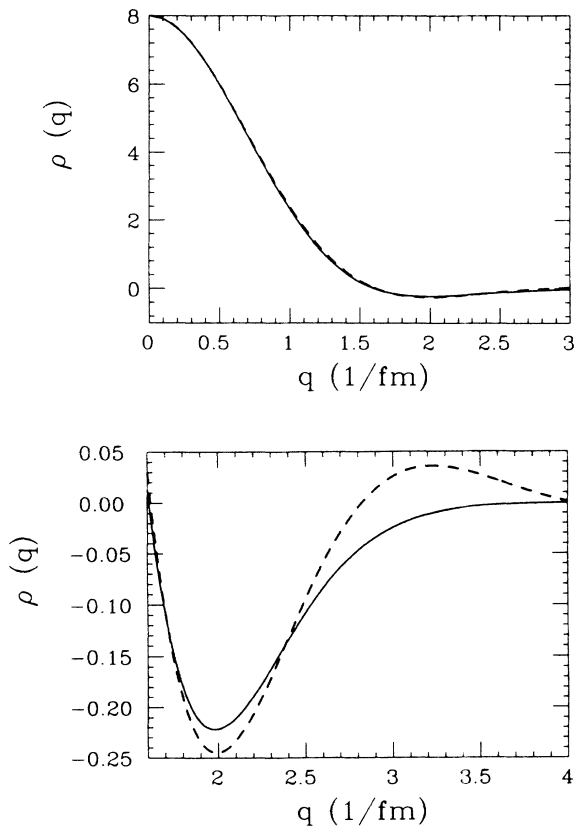

FIG. 2. Momentum-space density for the proton distribution of ^{16}O. The solid curve represents the harmonic oscillator model described in the text, the dashed curve is the three-parameter Fermi distribution of Ref. 19.

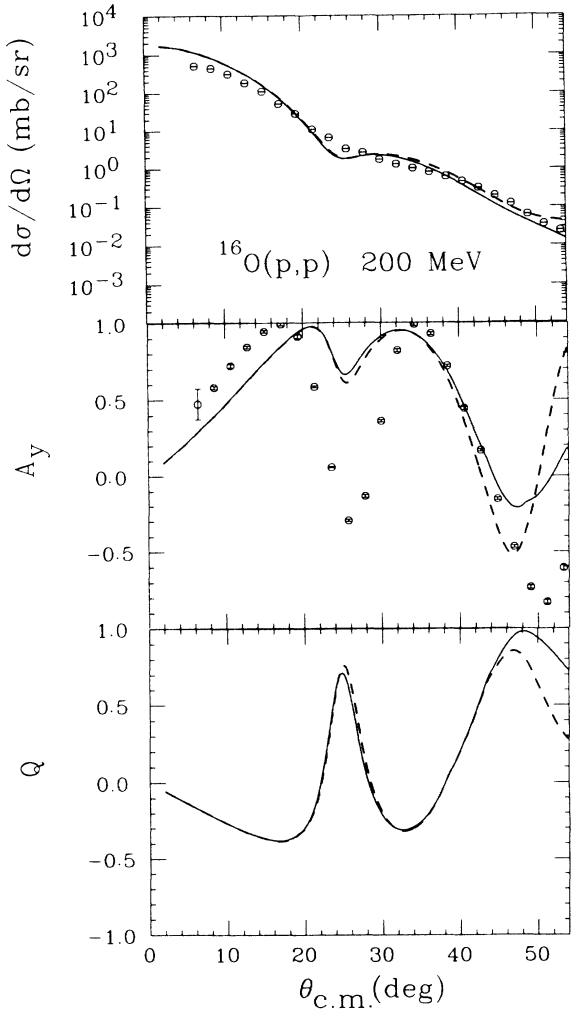

FIG. 3. The angular distribution of the differential cross section, analyzing power (A_y), and spin rotation function (Q) for elastic proton scattering from ^{16}O at 200 MeV laboratory energy. The calculations are with a first-order optical potential from the full Bonn interaction in the on-shell local approximation. The solid curve uses the oscillator model density, whereas the dashed curve represents a calculation with the three-parameter Fermi shape density from Ref. 19. The data are from Ref. 25.

scale of Fig. 2(b) shows that small deviations occur in the minimum and that the model density cannot fit the second zero at $q=2.8\ \mathrm{fm}^{-1}$.

In order to test the sensitivity of the differences in the two densities on the elastic scattering observables for proton scattering from ^{16}O, we calculated the angular distributions of the differential cross section, the analyzing power, (A_y), and the spin rotation function (Q) with a first-order optical potential based on the full Bonn interaction[14] in a local on-shell approximation. The results are displayed in Fig. 3. The dashed curve uses the three-parameter Fermi shape density of Ref. 19 whereas the solid curve is based on the model density of Eq. (15). The agreement between the two curves for angles smaller than 40° is very good. At larger angles deviations occur, which are reflections of the inadequacies of the oscillator model for higher q.

IV. FULL-FOLDING OPTICAL POTENTIAL FOR ^{16}O

Since ^{16}O is a spin saturated target, the required two-body t matrix reduces to a spin-independent component (corresponding to the Wolfenstein amplitude A) and to a spin-orbit component (corresponding to Wolfenstein amplitude C). The required t matrix can be written as

$$\tilde{t}_\alpha(\mathbf{q},\mathbf{Q};\varepsilon)=A(\mathbf{q},\mathbf{Q};\varepsilon)+i(\sigma_1+\sigma_2)\cdot\hat{\mathbf{n}}\,C(\mathbf{q},\mathbf{Q};\varepsilon)\ , \quad (16)$$

where $\mathbf{q}$ and $\mathbf{Q}$ are, respectively, the difference and average of the final and initial NN relative momenta and $\mathbf{n}=\mathbf{q}\times\mathbf{Q}$.

The evaluation of the full-folding potential of Eq. (6) can be simplified if we note that the two-body t-matrix has the following general characteristics.

(i) The off-shell Wolfenstein amplitudes A and C are only slowly varying functions of the two-particle scattering energy ε.[12] Consequently we can evaluate the Wolfenstein amplitudes at the fixed two-body scattering energy ε, which we choose to correspond to free NN scattering at the beam energy. It should be noted that the slow energy variation of the off-shell amplitudes does *not* mean that the on-shell amplitudes are energy independent. A great deal of the energy dependence comes from the on-shell constraint between $\mathbf{q}$ and $\mathbf{Q}$.

(ii) The off-shell amplitudes A and C' (where $C'=C/\sin\theta$) are nearly independent of the angle θ between $\mathbf{q}$ and $\mathbf{Q}$. In Ref. 12 this has been shown for the amplitudes derived from the Paris potential.[20] This finding is also true for other potentials based on a meson exchange model for the NN interaction.[6,14]

We can thus write

$$\tilde{t}_\alpha(\mathbf{q},\mathbf{Q};\varepsilon)=A(q,Q)+i(\sigma_1+\sigma_2)\cdot\hat{\mathbf{q}}\times\hat{\mathbf{Q}}\,C'(q,Q)\ , \quad (17)$$

where the dependence upon the fixed NN energy ε is to be understood. After integration over the density matrix the amplitude A leads to the central part of the optical potential, and C yields the spin-orbit part. Since the model density matrix employed does not distinguish protons and neutrons, the NN t matrix that enters is the average for pp and pn contributions. In the following, the NN amplitudes A and C are understood to be this average.

From Eq. (6) the central term of the full-folding (ff) optical potential is

$$\tilde{U}_{\mathrm{ff}}^{C}(q,K)=\frac{8}{(2\pi)^3}\left[\frac{A-1}{A}\right]\int dQ\,Q^2A(q,Q)\int d\Omega_Q\tilde{\rho}(q,|\mathbf{K}-2\mathbf{Q}|)\ . \quad (18)$$

After the angle integration is carried out, the s-shell density matrix given in Eq. (10) leads to the contribution

$$\tilde{U}_{\mathrm{ff}}^{C0}(q,K)=\left[\frac{A-1}{A}\right]\frac{4B_s}{\pi^2}e^{-(\alpha_s+\beta_s)}\int dQ\,Q^2A(q,Q)e^{-\gamma_s}\frac{\sinh\eta_s}{\eta_s}\ , \quad (19)$$

while the p-shell density matrix given in Eq. (12) leads to the contribution

$$\tilde{U}_{\mathrm{ff}}^{C1}(q,K)=\left[\frac{A-1}{A}\right]\frac{8}{3}\frac{B_p}{\pi^2}e^{-(\alpha_p+\beta_p)}\int dQ\,Q^2A(q,Q)e^{-\gamma_p}\left[(\alpha_p-\beta_p+\gamma_p+1)\frac{\sinh\eta_p}{\eta_p}-\cosh\eta_p\right]\ . \quad (20)$$

Here we have introduced the following abbreviations: $B_{s,p}=(4\pi/\nu_{s,p})^{3/2}$, $\eta_{s,p}=4KQ/\nu_{s,p}$, $\alpha_{s,p}=K^2/\nu_{s,p}$, and $\gamma_{s,p}=4Q^2/\nu_{s,p}$. The quantities $\beta_{s,p}$ are defined in Eq. (15). The total central part of the full-folding potential is then given by

$$\tilde{U}_{\mathrm{ff}}^{C}(q,K)=4\tilde{U}_{\mathrm{ff}}^{C0}(q,K)+12\tilde{U}_{\mathrm{ff}}^{C1}(q,K)\ . \quad (21)$$

It should be noted that $\tilde{U}_{\mathrm{ff}}^{C}$ is independent of the angle between $\mathbf{q}$ and $\mathbf{K}$ due to the simple density matrix employed.

For a spin-saturated 0^+ target $\langle\sigma_2\rangle\to 0$ and with the notation $\sigma_1\equiv\sigma$, the spin-orbit (LS) part of the optical potential obtained from Eq. (6) is

$$\tilde{U}_{\mathrm{ff}}^{\mathrm{LS}}(\mathbf{q},\mathbf{K})=8\left[\frac{A-1}{A}\right]\int\frac{d^3\mathbf{Q}}{(2\pi)^3}\frac{C'(q,Q)}{qQ}i\sigma\cdot\mathbf{q}\times\mathbf{Q}\tilde{\rho}(q,|\mathbf{K}-2\mathbf{Q}|)\ . \quad (22)$$

To facilitate the angular integration, we take $\hat{\mathbf{K}}$ as the polar axis and describe the orientation of $\hat{\mathbf{Q}}$ through $\xi=\hat{\mathbf{Q}}\cdot\hat{\mathbf{K}}$ and an azimuthal angle Φ. The azimuthal integration yields

$$\int_0^{2\pi} d\Phi\, \mathbf{q}\times\mathbf{Q}=2\pi\xi(\mathbf{q}\times\mathbf{K})Q/K \ . \tag{23}$$

We can thus make the factorization

$$\tilde{U}_{\rm ff}^{\rm LS}(\mathbf{q},\mathbf{K})=i\sigma\cdot\mathbf{q}\times\mathbf{K}\tilde{U}_{\rm ff}^{S}(q,K) \tag{24}$$

where the spin-orbit amplitude $\tilde{U}_{\rm ff}^{S}$ is independent of $\hat{\mathbf{q}}\cdot\hat{\mathbf{K}}$ and is given by

$$\tilde{U}_{\rm ff}^{S}(q,K)=-\left[\frac{A-1}{A}\right]\frac{2}{\pi^2}\int dQ\, Q^2\frac{C'(q,Q)}{qK}\int_{-1}^{1}d\xi\,\xi\tilde{\rho}(q,|\mathbf{K}-2\mathbf{Q}|) \ . \tag{25}$$

The contribution from the s-shell density matrix given in Eq. (10) is

$$\tilde{U}_{\rm ff}^{S0}(q,K)=\left[\frac{A-1}{A}\right]\frac{4B_s}{\pi^2 qK}\int dQ\, Q^2C'(q,Q)e^{-(\alpha_s+\beta_s+\gamma_s)}\frac{1}{\eta_s}\left[\frac{\sinh\eta_s}{\eta_s}-\cosh\eta_s\right] , \tag{26}$$

while the contribution of the p-shell density matrix given in Eq. (12) is

$$\tilde{U}_{\rm ff}^{S1}(q,K)=\left[\frac{A-1}{A}\right]\frac{8B_p}{3\pi^2 qK}\int dQ\, Q^2C'(q,Q)e^{-(\alpha_p+\beta_p+\gamma_p)}\left[\frac{1}{\eta_p}(\alpha_p-\beta_p+\gamma_p+2)\left[\frac{\sinh\eta_p}{\eta_p}-\cosh\eta_p\right]+\sinh\eta_p\right] . \tag{27}$$

The definition of the constants is the same as given in Eq. (20). The total spin-orbit part of the full-folding optical potential is then given by

$$\tilde{U}_{\rm ff}^{S}(q,K)=4\tilde{U}_{\rm ff}^{S0}(q,K)+12\tilde{U}_{\rm ff}^{S1}(q,K) \ . \tag{28}$$

The complete optical potential is thus

$$\tilde{U}_{\rm ff}(\mathbf{q},\mathbf{K})=\tilde{U}_{\rm ff}^{C}(q,K)+i\sigma\cdot\mathbf{q}\times\mathbf{K}\tilde{U}_{\rm ff}^{S}(q,K) \ . \tag{29}$$

The individual s-shell and p-shell contributions in Eqs. (19), (20), (26), and (27) are evaluated with standard Gaussian integration methods and the produced values are tabulated on a sufficiently fine grid of equally spaced points in the q-K space. The real parts of $\tilde{U}_{\rm ff}^{C}(q,K)$ and $\tilde{U}_{\rm ff}^{S}(q,K)$ from Eq. (29) for ^{16}O at 200 MeV scattering energy are displayed in Fig. 4(a). The corresponding real parts of the central and spin-orbit potential of the off-shell factorized approximation of Eq. (4) are shown in Fig. 4(b). The general tendency is that the full-folding potentials appear to be more local than the optimum factorized ones. By this we mean that the dependence on the gradient with respect to $\mathbf{K}$ is smaller for the full-folding potential. This is especially obvious in the real part of the central potential, where the optimum factor-

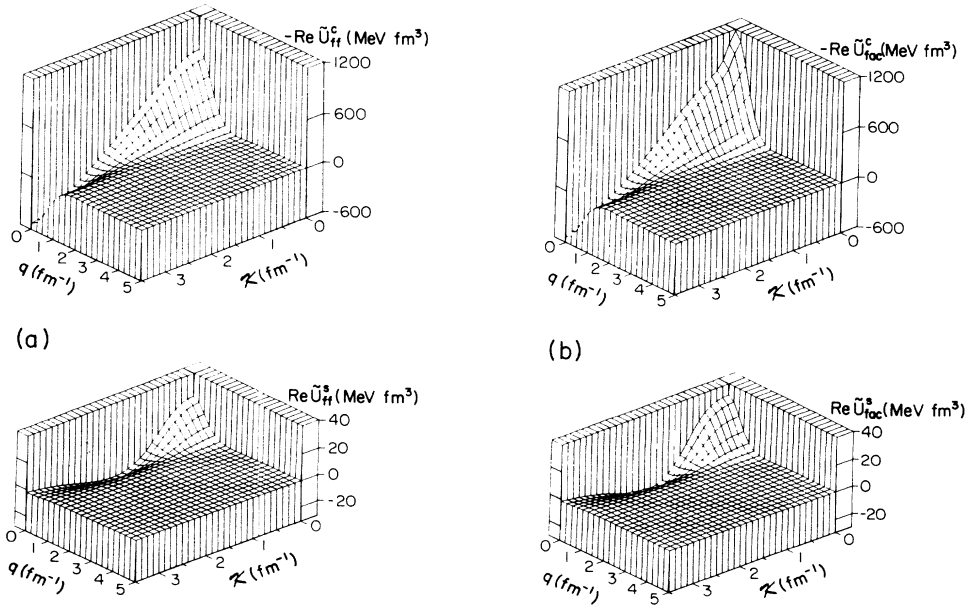

FIG. 4. Real parts of the central and spin-orbit potentials $\tilde{U}_{\rm ff}^{C}(\mathbf{q},\mathbf{K})$ and $\tilde{U}_{\rm ff}^{S}(\mathbf{q},\mathbf{K})$ as function of $\mathbf{q}$ and $\mathbf{K}$ for ^{16}O at 200 MeV laboratory energy. The potentials of the full-folding integration are displayed in (a), the ones obtained by the off-shell optimum factorization are shown in (b).

ized potential is about 30% more attractive in the interior than the full-folding potential.

V. ELASTIC SCATTERING RESULTS

We have carried out elastic scattering calculations[21] from ^{16}O at several energies between 100 and 500 MeV, to compare results obtained from the full-folding optical potential with those arising from the factorized off-shell and the local on-shell approximations. We do not draw definite conclusions from the comparison with experimental data because the simple harmonic oscillator density is inadequate at higher momenta. A second consideration is that in most calculations presented here we omit the Coulomb interaction, in order to isolate more precisely the effects resulting from treating the off-shell character of the full-folding optical potential and its approximations. We also omit recoil effects for calculational simplicity.

For 200 MeV scattering we employ the *NN t* matrix from the full Bonn interaction.[14] This includes the effects of relativistic kinematics, retarded meson propagators as given by time-ordered perturbation theory, and crossed and uncrossed meson exchanges with *NN*, *N*Δ, and ΔΔ intermediate states.

The scattering observables at 200 MeV are displayed in Fig. 5 with Coulomb effects omitted. The solid curve represents the calculation with the full-folding optical potential, the dashed line the off-shell optimum factorization, and the dotted line the on-shell local approximation. Since the former two calculations give similar results, it is apparent that the bulk of the nonlocality comes from the off-shell structure of the factorized *NN t* matrix. This can be especially seen in the spin observables A_y and Q, where the off-shell character of the *t* matrix changes the phase behavior of the observables. The full-folding optical potential produces little effect on the angular distribution of the differential cross section, but does deepen the interference minima of the spin observables.

We have extended the calculations to energies as low as 100 MeV and found that the character of the differences in the spin observables between the full-folding and the optimum factorized calculation is the same as at 200 MeV. Even at lower energies, the optimum factorization is found to be a good approximation to the full-folding integral.

In the work of Ref. 16 at 200 MeV the optimum factorization in terms of a fixed energy *t* matrix is found not to be such a satisfactory replacement for the full-folding integral. This may be due to the coupling of the effective energy of the *NN t* matrix to the momenta of the target density matrix that is included in that full-folding work. We keep this energy fixed for both the full-folding and factorized potentials so that the comparison will identify effects due only to the off-shell momentum dependence associated with the range of the *NN* force. The relevant downward energy shift that we have ignored for the *t* matrix consists of the single-particle binding energy (typically 20 MeV) and the deviations of the *NN* center-of-mass energy away from the most favored value which is half the beam energy. This latter shift is about $p^2/4m$, where p is a typical momentum supported by the single-particle bound states (about 1.4 fm^{-1}). The total downward energy shift of the *t* matrix away from the value corresponding to physical *NN* scattering at the beam energy should thus be at most 40 MeV. The behavior of the relevant off-shell *t*-matrix elements for values of the variables **q** and **Q** that dominate Eq. (6) is found to not be significantly altered by such an energy shift. This estimate may not be appropriate, however, for very high momentum components of the optical potential.

It is difficult to relate unambiguously the nonlocal property of a potential to the elastic scattering observables produced. In order to characterize how the potentials shown in Fig. 4 might influence the interior wave functions of the nucleus, we plot in Fig. 6 the real part of the phase shift δ as function of the orbital angular momentum L. We separate the cases $J=L+\frac{1}{2}$ and $J=L-\frac{1}{2}$ to isolate the effect of the spin-orbit force. We

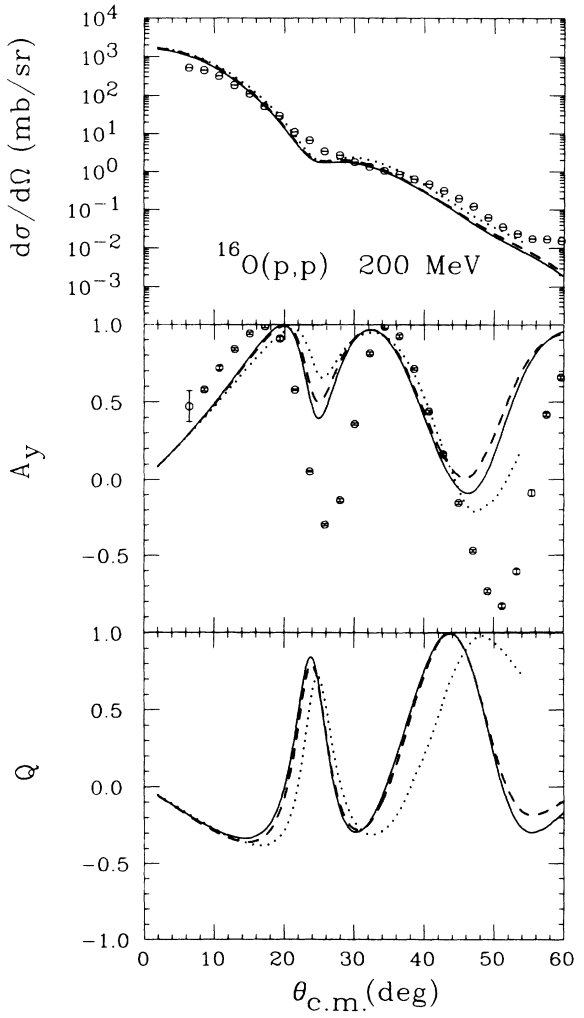

FIG. 5. Differential cross section A_y and Q for elastic proton scattering from ^{16}O at 200 MeV. The solid curve shows the calculation based on the full-folding optical potential, the dashed curve represents the factorized off-shell approximation, and the dotted line the local on-shell approximation. The data are from Ref. 25.

also show the absolute value of the S-matrix (η), that gives a measure of the absorptive character of the potentials in each partial wave. As is seen in Fig. 6, the full-folding and the optimum factorized potentials have nearly the same value of η in all partial waves, whereas the on-shell local potential is clearly more absorptive in lower partial waves. The real parts of the phase shifts show an increasing suppression for $L \leq 7$ as the nonlocal effects are treated more adequately. Because the absorption is relatively strong for these low partial waves, the elastic observables are not particularly sensitive to such refractive effects generated by the nonlocality.

In Fig. 7 we show the elastic scattering observables for ^{16}O at 200 MeV including Coulomb effects. Since an exact method for handling the Coulomb distortions in momentum-space scattering without problems in handling higher angular momentum states is presently not available, we employ the prescription developed in Ref. 4. There the Coulomb distorted nuclear bar phase-shifts are approximated by the pure nuclear phase shifts. The remaining effects, namely the multiplicative Coulomb partial wave S-matrix factor $e^{2i\sigma_l}$ and the additive pure Coulomb scattering amplitude, are included in the standard way. Figure 7 shows that the Coulomb effect enhances the difference between the calculations, especially in the spin observables for the full-folding and the optimum factorized optical potentials. Evidently the differences in the real parts of the interior phase shifts are modified by the factor $e^{2i\sigma_l}$, and the nonlocal effect is enhanced. This is especially clear at the interference minima.

For our scattering calculation at 500 MeV, we start from an extension of the Bonn meson exchange interaction above pion production threshold, which is described in more detail in Refs. 6 and 22. This NN model, called D52, contains iterative meson exchanges with NN, $N\Delta$, and $\Delta\Delta$ intermediate states. Pion production in this model is described through the decay of the delta isobar with a width obtained consistently from the imaginary part of the one-pion loop diagram for the delta self-energy. In Fig. 8 we show the scattering observables for elastic scattering from ^{16}O at 500 MeV laboratory energy with Coulomb effects omitted. The solid curve represents the calculation with the full-folding optical potential, the dashed curve the off-shell optimum factorized approximation, and the dotted curve the on-shell local approximation. As already shown at 200 MeV, most of the nonlocality effect is contained in the NN t matrix. In fact, the optimum factorization is an excellent approximation to the full-folding integral at 500 MeV. The off-shell effects evident in Fig. 8 from comparison of the two factorized approximations are smaller than those previously reported for this case by two of us in an earlier work.[6] This is due to the neglect of recoil effects and the use of the simple harmonic oscillator density in the present work. Both of these simplifications have been made to facilitate the full-folding integral. The present factorized calculations also include these simplifications for the sake of comparison. The earlier factorized results[6] for the same case as Fig. 8 contain larger off-shell effects at forward angles (especially in diffractive minima) due to the influence of recoil, while at angles beyond about 35°, the more realistic density employed previously has a significant impact on the observables. The clear trend from the present simplified investigation is that as the energy is raised the full-folding integral becomes better

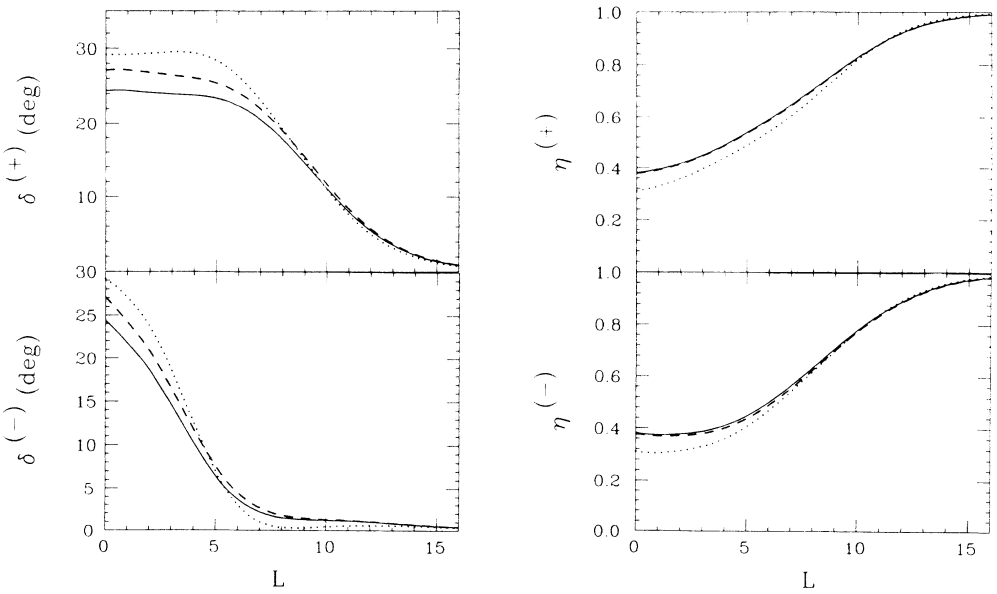

FIG. 6. Real part of the phase shift δ and absolute value of the S-matrix η as functions of the orbital angular momentum L for scattering from ^{16}O at 200 MeV laboratory energy. (+) denotes the phase shift for $J = L + \frac{1}{2}$, whereas (−) stands for $J = L - \frac{1}{2}$. The full-folding (solid), off-shell (dashed), and local on-shell (dotted) calculations are based on the full Bonn model in the first-order optical potential.

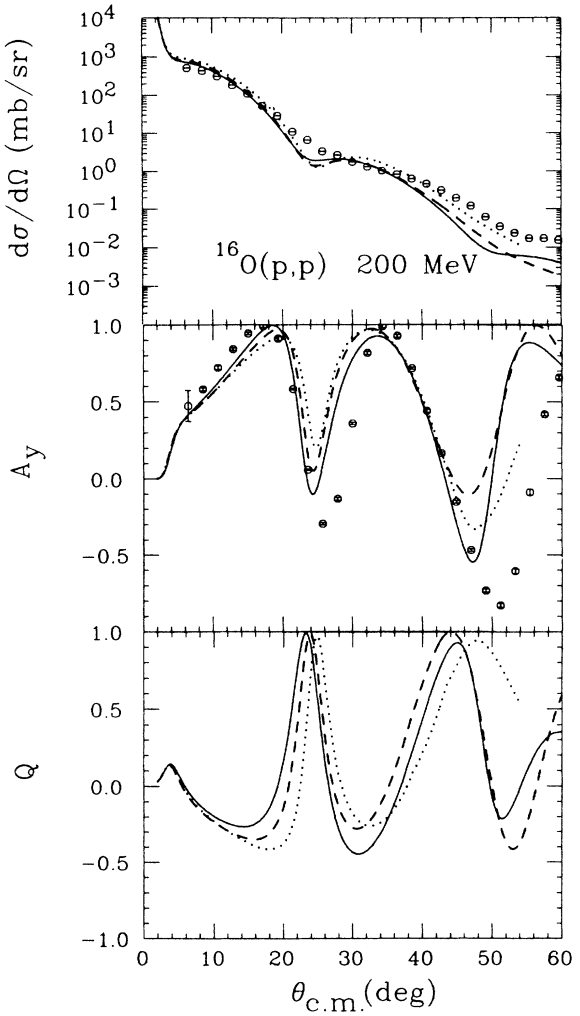

FIG. 7. Same as for Fig. 5, except that all calculations contain Coulomb distortions as described in the text.

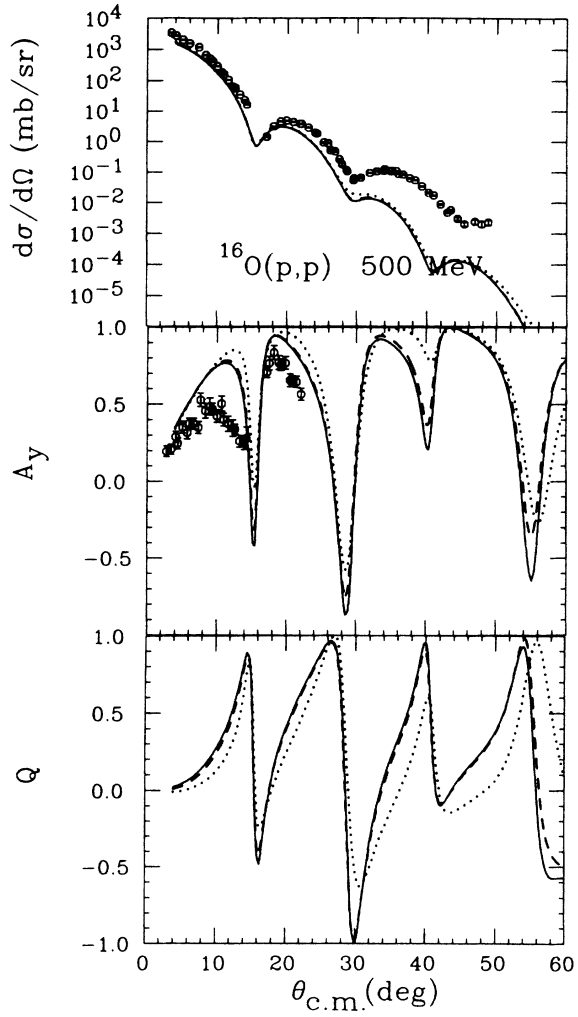

FIG. 8. Differential cross section A_y and Q for elastic proton scattering from ^{16}O at 500 MeV laboratory energy. The full-folding (solid), off-shell factorized (dashed), and local on-shell (dotted) calculations are based on the Bonn *NN* model D52 in the first-order optical potential. The data are from Ref. 25.

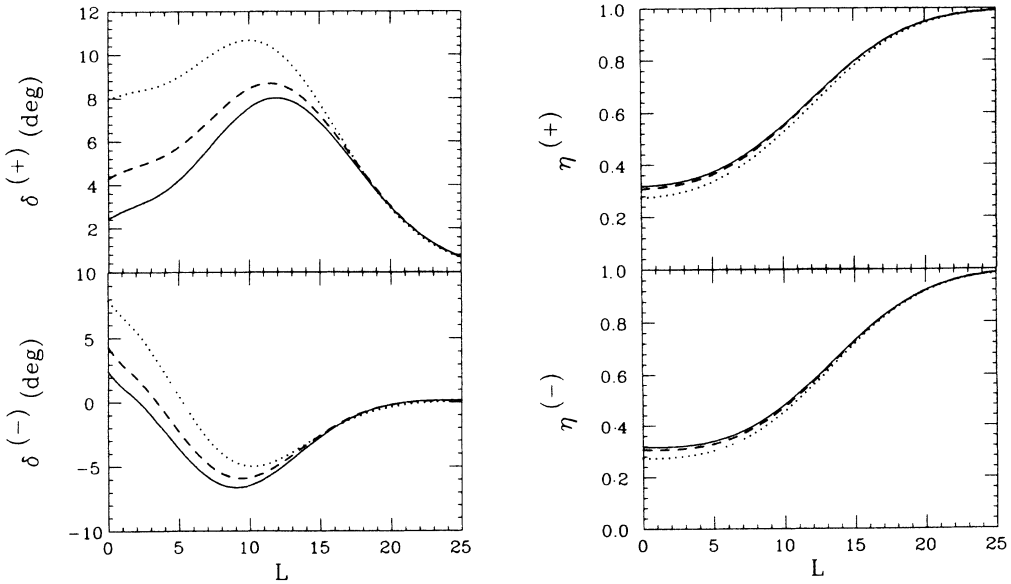

FIG. 9. Real part of the phase shift δ and absolute value of the *S*-matrix η as functions of the orbital angular momentum L for scattering from ^{16}O at 500 MeV laboratory energy. The notation is the same as in Fig. 6.

represented by the optimum factorized prescription. We have confirmed this through calculations up to 800 MeV. We would expect this trend to persist in the context of a more realistic density matrix.

In Fig. 9 we show the real part of the phase shift and the absolute value of the S matrix as a function of L for scattering at 500 MeV. Although the quenching of the real phase shift for small values of L ($L \leq 10$) with increasing nonlocality is more evident here than at lower energies, the strong absorption overcomes this effect in observables.

VI. APPROXIMATE LOCALIZATION AND EFFECTIVE MASS

The elastic scattering observables only measure the asymptotic properties of the scattering wave function. Inelastic scattering, transfer reactions, and knockout all require the elastic nucleon-nucleus wave function in the nuclear interior. Potentials with differing nonlocalities can agree in their elastic scattering observables and still have different interior wave functions. The nonlocality of the full-folding optical potential can have an impact on the results from distorted wave treatments in particular reaction channels.

The study of nonlocality in the nucleon optical model potential was initiated by Perey and Buck in the early 1960's.[15] They developed a perturbative scheme to approximate the nonlocal potential by a local one and identified a resulting damping factor for the interior wave function. A treatment of nonlocality of this type is helpful in identifying the underlying simple physics. Further efforts in studying nonlocal effects of the first-order optical potential were pursued in Refs. 5, 8, and 11. The interior damping factors of the Perey-Buck type are a useful device for characterizing both the nonlocality and the effects on interior wave functions.

In this section, we take an approach similar to that of Ref. 11 and formulate an approximate localization of the potential $\tilde{U}(\mathbf{q},\mathbf{K})$ by retaining the first two terms in the Taylor expansion in the variable K. The momentum-space matrix element of the effective nucleon-nucleus Hamiltonian is given by

$$H(\mathbf{q},\mathbf{K})=(2\pi)^3\delta^3(\mathbf{q})\frac{K^2}{2m}+\tilde{U}(\mathbf{q},\mathbf{K}) , \tag{30}$$

where the previously derived optical potential $\tilde{U}(\mathbf{q},\mathbf{K})$ has central and spin-orbit components and is given by

$$\tilde{U}(\mathbf{q},\mathbf{K})=\tilde{U}^C(q,K)+i\sigma\cdot\mathbf{q}\times\mathbf{K}\tilde{U}^S(q,K) . \tag{31}$$

To retain the lowest-order nonlocality of the amplitudes $\tilde{U}^C$ and $\tilde{U}^S$ we expand both of them in K about an arbitrary value K_0 to obtain

$$\tilde{U}^a(q,K)\simeq\tilde{U}^a(q,K_0)+(K^2-K_0^2)(2K_0)^{-1}\frac{\partial}{\partial K_0}\tilde{U}^a(q,K_0) , \tag{32}$$

where the superscript a stands for either C or S. As previously formulated, both of the amplitudes $\tilde{U}^C$ and $\tilde{U}^S$ are independent of the orientation of $\mathbf{K}$. The spin-orbit operator is not approximated and its full orientation properties are included.

In a coordinate space representation in which $\mathbf{r}'$ and $\mathbf{r}$ are the final- and initial-state positions of the projectile, the combination $\mathbf{R}=(\mathbf{r}'+\mathbf{r})/2$ is conjugate to $\mathbf{q}$ and $\mathbf{r}'-\mathbf{r}$ is conjugate to $\mathbf{K}$. After Fourier transformation from $\mathbf{q}$ space to $\mathbf{R}$ space where the relation

$$F(\mathbf{R},\mathbf{K})=\int\frac{d^3\mathbf{q}}{(2\pi)^3}e^{i\mathbf{q}\cdot\mathbf{R}}\tilde{F}(\mathbf{q},\mathbf{K}) \tag{33}$$

is applied to Eqs. (30)–(32), the K^2 terms of the potential may be combined with the kinetic-energy term to produce an effective mass. This yields the mixed representation for the Hamiltonian:

$$H(\mathbf{R},\mathbf{K})\simeq\mathbf{K}^2\frac{1}{2m^*(\mathbf{R})}+U(\mathbf{R},K_0)+K_0^2\left[\frac{1}{2m}-\frac{1}{2m^*(\mathbf{R})}\right] , \tag{34}$$

where $U(\mathbf{R},K_0)$ is defined by

$$U(\mathbf{R},K_0)=U^C(\mathbf{R},K_0)+\sigma\cdot\mathbf{R}\times\mathbf{K}\frac{1}{R}\frac{\partial}{\partial R}U^S(\mathbf{R},K_0) , \tag{35}$$

and the effective mass $m^*(\mathbf{R})$ is defined by

$$\frac{1}{2m^*(\mathbf{R})}=\frac{1}{2m}+\frac{1}{2K_0}\frac{\partial}{\partial K_0}U(\mathbf{R},K_0) . \tag{36}$$

The choice of expansion point K_0 is so far unspecified. It should be a value close to a typical average nucleon momentum in the scattering process. Obviously, the simplest choice is the asymptotic momentum K_0 which is defined by $K_0=\sqrt{2mE_{k_0}}$, where E_{k_0} is the beam energy.

After we Fourier transform Eq. (34) to convert the dependence upon $\mathbf{K}^2$ to a dependence upon $\mathbf{r}'-\mathbf{r}$, the Schrödinger equation

$$\int d^3r\,H\left[\frac{\mathbf{r}'+\mathbf{r}}{2},\mathbf{r}'-\mathbf{r}\right]\Psi(\mathbf{r})=E\Psi(\mathbf{r}') \tag{37}$$

will involve terms up to second order in derivatives of both $m^*(\mathbf{r})$ and $\Psi(\mathbf{r})$. With the definition

$$P(\mathbf{r},K_0)=\frac{m^*(\mathbf{r})}{m}=\left\{1+\frac{m}{K_0}\frac{\partial}{\partial K_0}\left[U^C(r,K_0)+\left[\frac{1}{r}\frac{\partial}{\partial r}U^S(r,K_0)\right]\sigma\cdot\mathbf{r}\times\frac{\nabla}{i}\right]\right\}^{-1} , \tag{38}$$

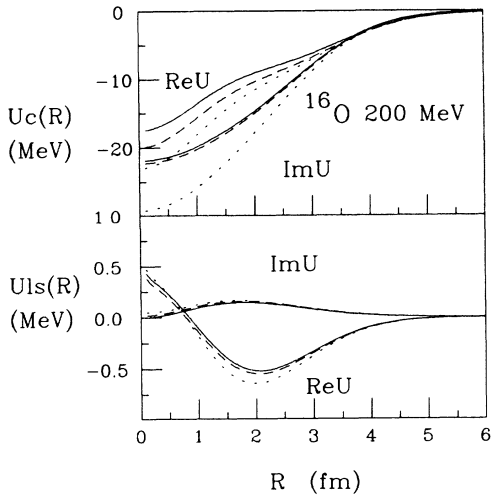

FIG. 10. Real and imaginary parts of the approximate local potentials for ^{16}O at 200 MeV laboratory energy. The solid curve is the local approximation to the full-folding optical potential, the dashed curve the local approximation to the off-shell optimum factorized optical potential, and the dotted line is representative of the on-shell local potential.

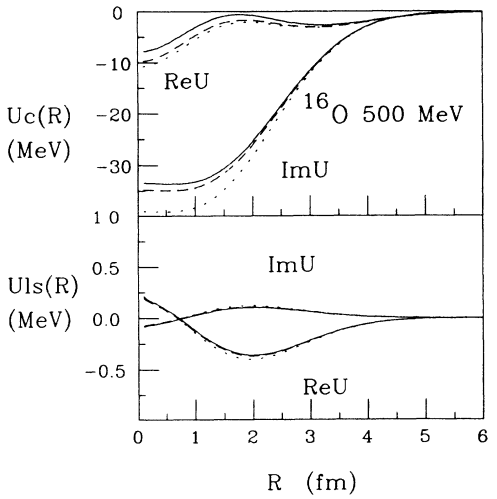

FIG. 11. Real and imaginary parts of the approximate local potentials for ^{16}O at 500 MeV laboratory energy as discussed in Sec. VI. The notation is the same as in Fig. 10.

and the introduction of an associated wave function $\Phi(\mathbf{r})$ defined by

$$\Psi(\mathbf{r})=\sqrt{P(\mathbf{r},K_0)}\Phi(\mathbf{r}) , \tag{39}$$

the first-order derivatives of $\Psi(\mathbf{r})$ are eliminated. The resulting Schrödinger equation is

$$\left[-\frac{1}{2m}\nabla^2+P(\mathbf{r},K_0)U(\mathbf{r},K_0)\right]\Phi(\mathbf{r})=E\Phi(\mathbf{r}) , \tag{40}$$

where we have neglected terms of second order in derivatives of $P(\mathbf{r},K_0)$. The factor P is the Perey factor, which exhibits the damping of the wave function in the nuclear interior due to the nonlocality of the original optical potential. The effective local potential associated with $\Phi(\mathbf{r})$ is given by

$$U_{\rm loc}(\mathbf{r},K_0)=P(\mathbf{r},K_0)U(\mathbf{r},K_0) . \tag{41}$$

Slight differences in the choice of K_0 do not seriously affect the resulting local potential $U_{\rm loc}$. Our calculations confirm this point.

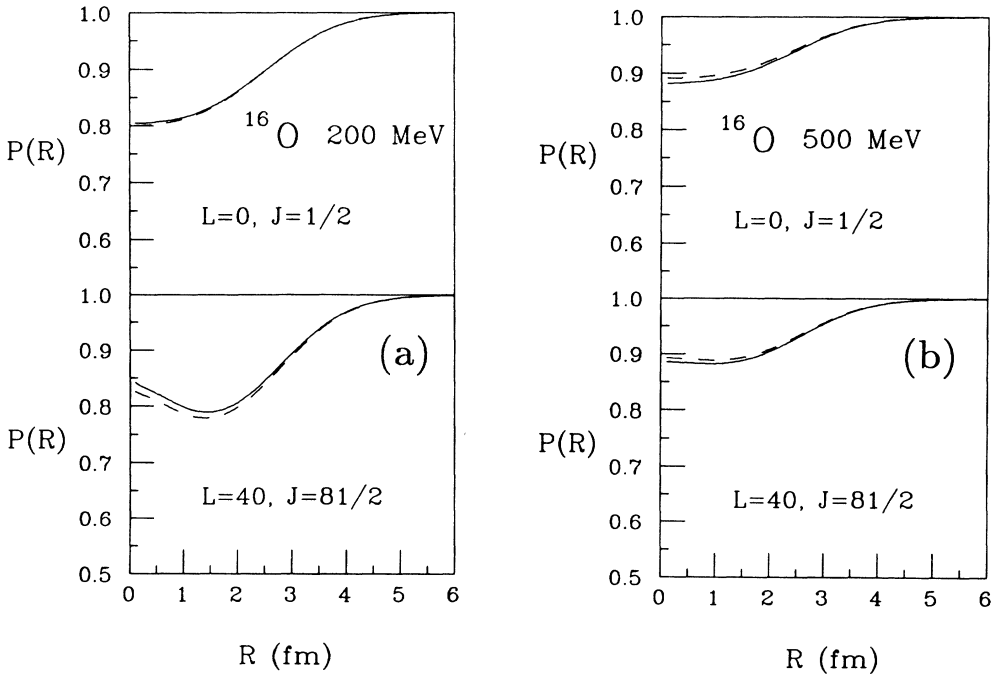

FIG. 12. Real part of the Perey damping factor as given in Eq. (38) for ^{16}O at 200 MeV (a) and at 500 MeV (b) for $L=0$ and 40. The solid curve is due to the full-folding optical potential, whereas the dashed curve is derived from the optimum factorized optical potential.

In Figs. 10 and 11 we show the effective local potentials $U_{\rm loc}$ calculated from the nonlocal potentials of the previous section for proton-oxygen scattering at 200 and 500 MeV. The solid and dashed curves represent the localized versions of the full-folding potential and the optimum factorized potential, respectively. The dotted curve is also obtained from the optimum factorized potential except that the Perey factor $P(r)$ is set to unity. This removes the principal nonlocal effects and corresponds closely to the original on-shell local optical potential. The correspondence is not exact because of the fixed value of K_0 that is employed here instead of the q-dependent condition for the on-shell limit of the NN t matrix [as discussed after Eq. (4)].

In Fig. 12 the real part of the Perey factor as defined in Eq. (38) is displayed for both energies. The figures show the factor $P(\mathbf{r},K_0)$ for the S wave and for a peripheral wave. The value of the real part of the Perey factor at the nuclear center is about 0.8 at 200 MeV which is consistent with an earlier estimate for the type of optical potential treated here.[23,24] The imaginary part of $P(\mathbf{r},K_0)$ is very small. Its peak value at the nuclear center is about 0.02–0.03. In all calculations of observables, both real and imaginary parts are included. The scattering observables calculated from these approximate local potentials are plotted in Figs. 13 and 14. In each graph, the solid line is the result from the localized full-folding potential while the long dashed and dotted lines are from the localized optimal factorization with and without the

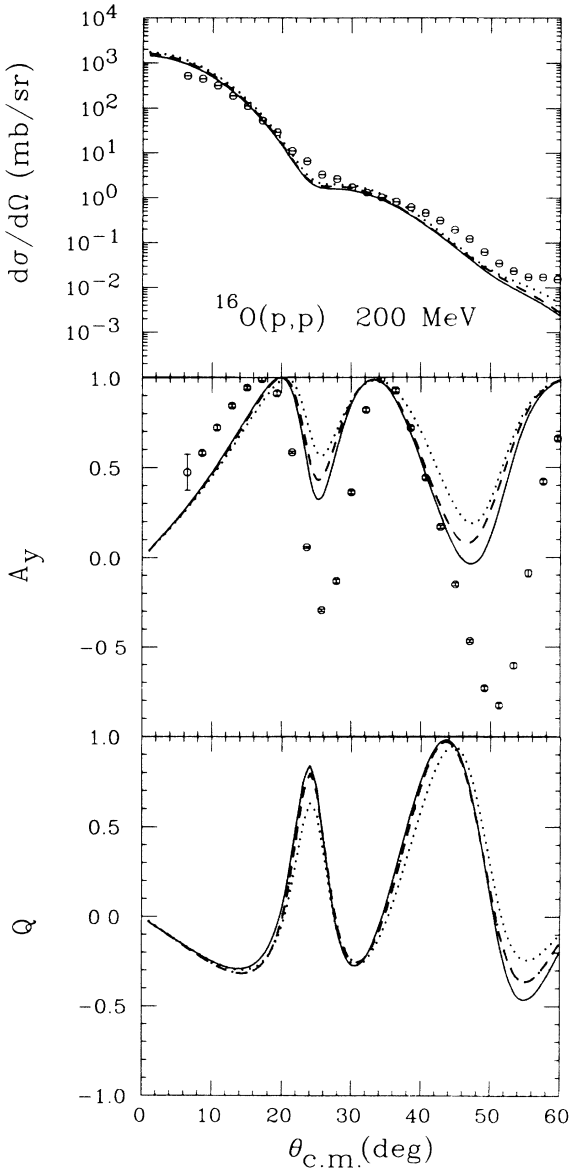

FIG. 13. Differential cross section A_y and Q for elastic proton scattering from ^{16}O at 200 MeV laboratory energy. All calculations are based on the local equivalent treatment of the optical potentials as discussed in Sec. VI. The solid line corresponds to the full-folding, the dashed line to the optimum factorized, and the dotted line to the on-shell local optical potential. These calculations are to be compared to the full calculations shown in Fig. 5.

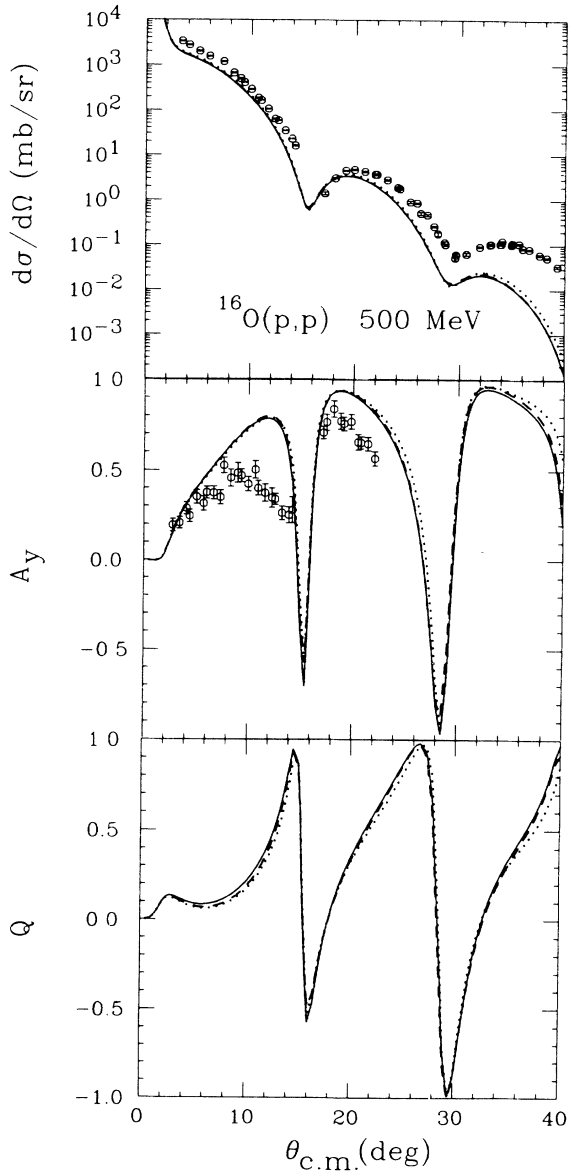

FIG. 14. Differential cross section A_y and Q for elastic proton scattering from ^{16}O at 500 MeV. The calculations are based on the local equivalent optical potentials of Sec. VI and to be compared to the full calculations of Fig. 8. The notation is the same as in Fig. 13.

Perey factor, respectively. A comparison of these results with the results from the original potentials (Figs. 5 and 8) shows that the approximate localization carried out here retains the dominant effects of the original nonlocality especially at forward angles. The calculation and use of the Perey damping factor for full-folding potentials can, to a large extent, summarize the reduction of the associated nonlocal wave equation to a convenient local form.

VII. SUMMARY AND CONCLUSIONS

We have investigated the accuracy of factorization approximations that are usually employed to calculate the single-scattering term of the nonrelativistic nucleon-nucleus optical potential. The complete full-folding integral for this first-order optical potential has been carried out with the simplifying assumption that the density matrix for ^{16}O is given by a simple harmonic oscillator model. Without the factorization of an appropriate NN t-matrix element from the full-folding integral, one is faced with a very large calculation in order to properly treat the complicated coupling between the t matrix and the off-diagonal one-body density matrix for the target nucleus. An *ad hoc* prescription for avoiding this complexity can misrepresent the intrinsic nonlocality present in the theory. It is important to retain the dominant nonlocality in approximate procedures not only for the task of obtaining elastic phase shifts that are an accurate reflection of the simple first-order theory, but also to obtain accurate elastic scattering wave functions inside the nuclear environment for future application in distorted wave treatments of reactions such as inelastic excitations and nucleon knockout.

For elastic nucleon-nucleus scattering at intermediate energies, we find that the effects of the intrinsic nonlocality of the complete full-folding first-order optical potential are extremely well accounted for by the optimum factorization procedure. Here a particular off-shell NN t-matrix element is identified as the best object to remove from the integral. The integral then recovers the diagonal (local) single-particle density. This result leads to the conclusion that of the two sources of nonlocality in the problem, the t matrix and the off-diagonal density matrix, the former is dominant for elastic observables.

We have confirmed that even for energies as low as 100 MeV the full-folding optical potential can be safely replaced by the optimum factorized potential with little loss of accuracy. Of course, at such low energies the physical relevance of a first-order optical potential theory in terms of a free space NN t matrix is in doubt due to the importance of medium effects related to Pauli blocking as demonstrated elsewhere. However, if the t matrix is replaced by an in-medium g matrix, the same question of the appropriateness of a factorization prescription arises in practice. If the dependence of the g matrix upon the variables θ and ε is as weak as is found for the t matrix, then our results here imply that the optimum factorization of a similarly defined off-shell momentum matrix element of the NN g matrix would be required to take proper account of the intrinsic nonlocal effects on the elastic observables. At low energies, the g matrix is known to be less sensitive to the energy variable than is the t matrix. This needs to be investigated for intermediate energy. Finite nucleus effects should be included in such an investigation since the dependece of the g matrix upon the total momentum of the interacting pair must be dealt with. This dependence is trivial for the free t matrix (a delta function), but can be quite complicated for a finite nucleus g matrix.

Much of the work reported here has been concerned with the assessment of whether a factorization approximation retains the dominant nonlocal effect upon elastic wave functions interior to the nucleus compared to the use of the more exact full-folding potential. Unfortunately such information is distributed over many angular momentum components and the net effect is an aggregate of delicate phase behavior. A further complication is that due to surface dominance of elastic scattering, the elastic observables can be insensitive to a nonlocality that modifies the low angular components of the wave function. This is evident in the figures that display the phases and magnitude of the S matrix as a function of the orbital angular momentum.

To obtain a better characterization of the effects on the interior wave function, we convert the nonlocal potentials to approximate local ones through a first-order Taylor expansion in the momentum variable that carries the nonlocal behavior. This converts the nonlocality into a variable effective mass for the nucleon projectile after the spirit of the analysis first performed by Perey and Buck. The result of this analysis is the identification of a Perey damping factor (the ratio of effective mass to bare mass) that describes the suppression of the interior wave function due to nonlocality in the original potential. The Perey factors are largely independent of angular momentum and our results strongly suggest that the optimum factorized potentials reproduce the dominant nonlocal suppression on the interior wave functions that comes from the more correct full-folding potential. The effective mass extracted here comes entirely from the nonlocality of the free effective NN interaction. No many-body effects have been included in this calculation.

Besides the extraction of Perey factors, the approximately localized version of the scattering problem detailed here is of practical utility. The elastic observables obtained from the effective local wave equation give a good account of the observables obtain from the nonlocal potentials. Evidently one can arrange an effective mass to carry most of the burden of the nonlocality of first-order optical potentials. It is hoped that the results from this work can help in the task of incorporating the effects from nonlocal first order optical potentials into distorted wave treatments of reactions via realistic elastic wave functions.

ACKNOWLEDGMENTS

B.C. Clark, R.J. Perry, and R.M. Thaler are thanked for stimulating discussions and reading of the manuscript. The authors acknowledge financial support from the Battelle Memorial Institute, the National Sci-

ence Foundation under Grant Nos. PHY87-19526, PHY88-58350, PHY85-05736, and PHY88-05633, and the Department of Energy under Grant No. DE-FG05-87ER-40322. The computational support of the Ohio Supercomputer Center under Grant No. PGS070, the Physics Department of the Ohio State University, the San Diego Supercomputer Center, and the University of Maryland Computer Science Center is gratefully acknowledged.

[1]J. A. McNeil, J. Shepard, and S. J. Wallace, Phys. Rev. Lett. **50**, 1443 (1983); B. C. Clark, S. Hama, R. L. Mercer, L. Ray, and B. D. Serot, Phys. Rev. Lett. **50**, 1644 (1983).

[2]M. V. Hynes, A. Picklesimer, P. C. Tandy, and R. M. Thaler, Phys. Rev. Lett. **52**, 978 (1984); Phys. Rev. C **31**, 1438 (1985).

[3]J. P. Jeukenne, A. Lejeune, and C. Mahaux, Phys. Rep. **25**, 83 (1976).

[4]A. Picklesimer, P. C. Tandy, R. M. Thaler, and D. H. Wolfe, Phys. Rev. C **29**, 1582 (1984); **30**, 1861 (1984).

[5]T. Cheon, Phys. Rev. C **35**, 2225 (1987).

[6]Ch. Elster and P. C. Tandy, Phys. Rev. C **40**, 881 (1989).

[7]M. MacFarlane and E. F. Redish, Phys. Rev. C **37**, 2245 (1988).

[8]E. J. Moniz, Phys. Rev. C **7**, 1750 (1973).

[9]R. H. Landau, Ann. Phys. (N.Y.) **92**, 205 (1973).

[10]D. J. Ernst, G. A. Miller, and D. L. Weiss, Phys. Rev. C **27**, 2733 (1983).

[11]T. Cheon, Phys. Rev. C **37**, 1088 (1988); **38**, 1516 (1988).

[12]E. F. Redish and K. Stricker-Bauer, Phys. Rev. C **35**, 1183 (1987).

[13]E. F. Redish, in *Antinucleon- and Nucleon-Nucleus Interactions* (Plenum, New York, 1985), p. 213.

[14]R. Machleidt, K. Holinde, and Ch. Elster, Phys. Rep. **149**, 1 (1987).

[15]F. Perey and B. Buck, Nucl. Phys. **32**, 353 (1962).

[16]H. F. Arellano, F. A. Brieva, and W. G. Love, Phys. Rev. Lett. **63**, 605 (1989).

[17]A. K. Kerman, H. McManus, and R. M. Thaler, Ann. Phys. (N.Y.) **8**, 551 (1959).

[18]P. C. Tandy, E. F. Redish, and D. Bollé, Phys. Rev. C **16**, 1924 (1977).

[19]C. W. DeJager, M. De Vries, and C. De Vries, Nucl. Data Tables **14**, 479 (1974).

[20]M. Lacombe *et al.*, Phys. Rev. C **21**, 861 (1980).

[21]All scattering calculations presented here contain an additional factor in the optical potential to account for the transformation of the *NN t* matrix from the two-nucleon c.m. frame to the nucleon-nucleus c.m. frame. This Möller factor is obtained in the manner discussed in Ref. 4.

[22]Ch. Elster, PhD. thesis, University of Bonn, 1986.

[23]C. Mahaux, B. F. Bortignon, R. A. Broglia, and C. H. Dasso, Phys. Rep. **120**, 1 (1985).

[24]T. Cheon and Ch. Elster, Prog. Theor. Phys. **81**, 559L (1989).

[25]C. Chan, M. S. thesis, University of Alberta, 1985; D. Hutcheon, private communication.